Vortex motions in coupled phase oscillator lattices with inertia under shear stress

Hidetsugu Sakaguchi
Interdisciplinary Graduate School of Engineering Sciences, Kyushu University, Kasuga, Fukuoka 816-8580, Japan

(Received 26 November 2021; accepted 8 May 2022; published 20 May 2022)

We propose a coupled phase oscillator model with inertia and study the vortex motion in the model when the external force is applied at the boundaries. The vortex exhibits a glide motion when the external force is larger than a critical value. We find a transition from the pair annihilation to passing for the collision of the vortex and antivortex when the external force is changed. In the parameter range of the passing, a single vortex exhibits a reciprocal motion, which leads to desynchronization. When the external force is further increased, the multiplication of vortices occurs and the jump of the frequency profile increases. The desynchronization induced by the vortex motion is analogous to the plastic flow induced by the dislocation motion under the shear stress in solids. In perfect crystals without dislocations, the plastic flow hardly occurs. We further show that a vortex ring is generated when a vortex line passes through an impurity region, which corresponds to the Orowan loop in the theory of plasticity.

DOI: 10.1103/PhysRevE.105.054211

I. INTRODUCTION

Coupled limit-cycle oscillators and mutual synchronization have been investigated in various research fields such as physics, chemistry, biology, and electric engineering [1–3]. The coupled phase oscillators called the Kuramoto model have been intensively studied by many authors as a simple solvable model [1,4–6]. In the phase oscillator models, the dynamics of limit-cycle oscillators are expressed with the phase of the oscillation. Various types of phase oscillator models have been proposed since the original Kuramoto model [7]. One generalized model includes the inertia term or the second derivative of the phase variable [8]. The phase oscillator model with inertia was applied to the power grid, where the alternating current is expressed using its phase [9,10]. The original Kuramoto model has a global coupling and the mean-field approximation can be applied exactly. However, coupled phase oscillators on square or cubic lattices are also important, which are called oscillator lattices [11,12]. For example, a two-dimensional oscillator lattice has a form

$$\frac{d\phi_{i,j}}{dt} = K\sum_{i',j'} \sin(\phi_{i',j'} - \phi_{i,j} + \alpha),$$

where $\phi_{i,j}$ is the phase of the oscillator on a lattice site (i, j), and (i', j') denotes the nearest-neighbor site of the (i, j) site, K is the coupling strength, and α is a parameter of the phase shift. Target and spiral waves appear on the oscillator lattices with nonzero α, which is similar to the phenomena observed in the oscillatory reaction-diffusion equations. In the center of the spiral, there exists a topological defect called a vortex [13].

Strongly deformed solids exhibit various nonlinear phenomena such as fractures in brittle materials and plastic flow in ductile materials. Defects such as micro cracks and dislocations play an essential role in the large deformation of solids. Perfect crystals without such defects are considered to be much stronger. The mechanics of plasticity is one of the basic research fields of solid materials. Many dislocations exist in strongly deformed materials. The screw and edge dislocations are typical line defects in crystals. The dynamics of dislocations is a fundamental process in the mechanics of plasticity [14,15]. The dislocation motions have been numerically studied with the molecular dynamics simulation. Several authors developed direct numerical simulation methods of the dislocation lines [16,17].

The dislocation motion has been studied from a viewpoint of nonlinear physics. The Frankel-Kontorova model is a simple one-dimensional model of dislocation motion [18,19]. The continuum approximation of the Frenkel-Kontorova model becomes the sine-Gordon equation, which is known as an integrable system. Although the original model is a conservative system, a dissipative system can be constructed by adding a viscous term. The Frenkel-Kontorova model is generalized to a two-dimensional system by several authors [20]. The two-dimensional Frenkel-Kontorova model is expressed as

$$\frac{d^2u_{i,j}}{dt^2} = -\sin u_{i,j} + K\sum_{i',j'}(u_{i',j'} - u_{i,j}),$$

where $u_{i,j}$ denotes the displacement of a particle at the (i, j) site.

The phase oscillator model on lattices and the lattice dynamics of crystals have several things in common. If the phase in the phase oscillator lattice is interpreted as the one-dimensional displacement from the equilibrium position in crystals, the vortex in the phase oscillator lattice corresponds to the dislocation in crystals. The shear stress is applied for the deformation in solids. The shear stress is expressed as an external force on the boundaries in the phase oscillator lattice.

 ©2022 American Physical Society

The average velocity in the plastic motion corresponds to the average frequency of the phase oscillator.

The complex dynamics such as chaos and defect turbulence has not been well studied in the research field of dislocation theory. On the other hand, the nonlinear response to the external force such as the shear stress has not been studied in oscillator lattices. We will propose a phase oscillator lattice model with inertia and study the complex dynamics of vortices and vortex lines in the oscillator lattices by applying the force corresponding to the shear stress. We will show various nontrivial dynamical phenomena with numerical simulations. The main result is the desynchronization induced by the vortex motion.

The vortex motion is studied on two-dimensional lattices in Sec. II and on three-dimensional lattices in Sec. III. Spontaneous creation of vortices and vortex rings in oscillator lattices with impurities is studied in Sec. IV. In Sec VI, we study an interaction of a vortex line and an impurity region. In Sec. VII, we summarize numerical results of our phase oscillator lattices.

II. VORTEX MOTIONS IN COUPLED PHASE OSCILLATORS ON SQUARE LATTICE

We study coupled phase oscillators with inertia on the square lattice in this section. Our coupled phase oscillator model with inertia is expressed as

$$\frac{d^2\phi_{i,j}}{dt^2} = K\sum_{i',j'}\sin(\phi_{i',j'}-\phi_{i,j}) - d\frac{d\phi_{i,j}}{dt} + f_{i,j}, \quad (1)$$

where (i', j')'s are the four nearest-neighbor sites of the (i, j) site on the rectangular lattice of $L_x \times L_y$, K is the coupling constant, and d is a parameter of the viscous resistance. The no-flux boundary conditions are imposed at $i = 1, i = L_x, j = 1$, and $j = L_y$ in most numerical simulations in this paper. This model equation is simple but not well studied, although there are many model equations closely related to this equation.

If $d = 0$, $f_{i,j} = 0$, and the phase difference $\phi_{i',j'} - \phi_{i,j}$ is sufficiently small, the continuum approximation of Eq. (1) is expressed as

$$\frac{\partial^2\phi}{\partial t^2} = K\left(\frac{\partial^2\phi}{\partial x^2} + \frac{\partial^2\phi}{\partial y^2}\right). \quad (2)$$

This equation has the form of the equation of motion of the two-dimensional elastic body when the displacement is assumed to be $(0, 0, \phi)$. The parameter K corresponds to μ/ρ, where μ is the modulus of rigidity and ρ is the density of the elastic body.

As a model of the shear stress, the external force $f_{i,j}$ is applied at the boundaries in the y direction as $f_{i,j} = F$ at $j = L_y$ and $f_{i,j} = -F$ at $j = 1$. The external force $f_{i,j}$ is set to be zero for the other lattice points. The numerical simulations were done using the fourth-order Runge-Kutta method with time step $\Delta t = 0.005$. Our model has three control parameters: K, d, and F. F is a parameter of the external force and K denotes the rigidity. The response of the system is mainly determined by F/K. The parameter d denotes the dissipation rate and the vortex dynamics changes by d qualitatively. If the initial condition is uniform, such as $\phi_{i,j} = 0$, a stationary solution is obtained if K is smaller than a critical value. Figure 1(a) shows a stationary profile of $\phi_{i,j}$ at the cross section $i = L_x/2$ for $K = 1$, $d = 0.2$, and $F = 0.5$ in a system of 20×20. The stationary solution $\phi_{i,j}$ satisfies

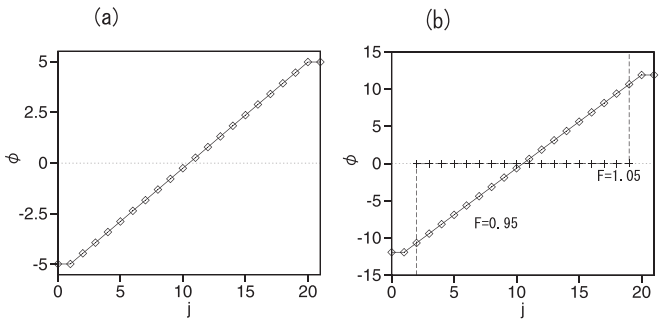

FIG. 1. (a) Stationary profile of $\phi_{i,j}$ at $i = L_x/2$ at $K = 1$, $F = 0.5$, and $d = 0.2$. (b) $\phi_{i,j}$ at $i = L_x/2$, at $F = 0.95$, and 1.05 for $K = 1$ and $d = 0.2$.

$$\phi_{i,j} = \Delta\{j - (L_y + 1)/2\}. \quad (3)$$

The coefficient Δ is given by $\Delta = \sin^{-1}(F/K)$ because

$$K\{\sin(\phi_{i,L_y+1} - \phi_{i,L_y}) + \sin(\phi_{i,L_y-1} - \phi_{i,L_y})\} = -K\sin(\Delta) + F = 0 \quad (4)$$

is satisfied at $j = L_y$. If $F > K$, there is no solution for Δ and the desynchronization occurs. Figure 1(b) shows the profile of $\phi_{i,j}$ at $i = L_x/2$ at $F = 0.95$ and $F = 1.05$ for $K = 1$ and $d = 0.2$. At $F = 0.95$, there is a stationary profile with $\Delta = \sin^{-1}(0.95) \sim 1.25$. However, the desynchronization occurs between $j = L_y$ and $j = L_y - 1$ and between $j = 1$ and $j = 2$ at $F = 1.05$. The phase ϕ_{i,L_y} increases with time and the profile of $\phi_{i,j}$ between $j = 2$ and $L_y - 1$ becomes rather flat. The critical value of the desynchronization is $F_c = K$.

If a defect called a vortex exists initially, the result changes drastically. To set a vortex as an initial condition, the phase profile is assumed to be

$$\phi_{i,j} = \cos^{-1}(y/r) \text{ for } x < 0, \text{ and}$$
$$\phi_{i,j} = 2\pi - \cos^{-1}(y/r) \text{ for } x > 0,$$

where $x = i - (L_x + 1)/2$, $y = j - (L_y + 1)/2$, and $r = \sqrt{x^2 + y^2}$. Figure 2 shows the vector $(\cos\phi_{i,j}, \sin\phi_{i,j})$ at each lattice position. There is a phase singularity or a vortex at $x = y = 0$. If the direction $(\cos\phi_{i,j}, \sin\phi_{i,j})$ rotates anticlockwise (clockwise) by one turn when we circulate anticlockwise around the defect, the defect is called a vortex (antivortex). This phase configuration corresponds to the displacement of the screw dislocation of the Burgers vector $(0, 0, 2\pi)$, if $\phi_{i,j}$ is interpreted as the displacement in the z direction. The Burgers vector is a vector that represents the lattice distortion for the dislocation. If the shear stress is applied to the crystal, the dislocation is considered to move in a periodic potential called the Peierls potential, which is caused by the periodic structure of the crystal. The minimum force necessary for the dislocation to go over the potential peak is called the Peierls stress. The Peierls stress is much smaller than the critical stress for the yielding in perfect crystals. That is why the dislocation is important to determine the mechanical property of the solid.

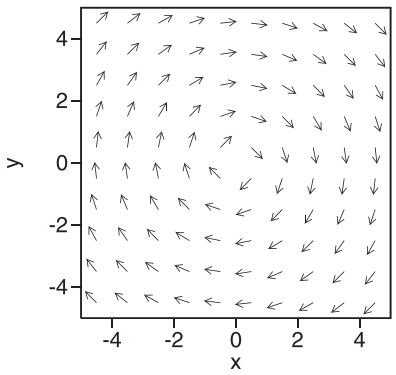

FIG. 2. Phase configuration of a vortex.

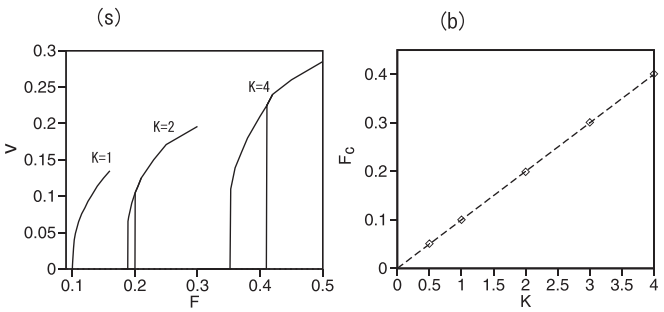

FIG. 4. (a) Average velocity as a function of F at $K = 1$, 2 and 4 for $d = 0.2$. (b) Critical value F_c as a function of K for $d = 0.2$.

By the analogy to the dislocation motion, the vortex is expected to move in our oscillator lattice if the external force F is beyond a critical value.

Figure 3(a) shows the time evolution of the x coordinate of the vortex position at $F = 0.1018$ and 0.15 for $K = 1$ and $d = 0.2$. The system size is 500×100. The position of the vortex can be determined as a lattice site with nonzero local vorticity along the square loop $(i, j) \to (i+1, j) \to (i+1, j+1) \to (i, j+1) \to (i, j)$. At $F = 0.15$, the vortex moves in the x direction almost with a steady velocity after an initial transient time. That corresponds to the glide motion of the dislocation. The y coordinate of the position of the vortex is fixed to be $L_y/2$. At $F = 0.1018$, a stick-slip motion is observed. The stick-slip motion is observed for a small parameter range of $0.1002 \leqslant F \leqslant 0.1032$ at $d = 0.2$. The period of the stick-slip oscillation increases with F and the time interval of the stick state decreases with F, however, any singularity such as divergence is not observed. Figure 3(b) shows a relationship between F and the time interval ST of the stick state for $K = 1$ and $d = 0.2$. A discontinuous transition seems to occur at $F = 0.10323$. To study the robustness of the stick-slip motion, we have performed numerical simulations with external noises $f_{i,j}(t)$ satisfying $\langle f_{i,j}(t) f_{i',j'}(t')\rangle = 2D\delta_{i,i'}\delta_{j,j'}\delta(t-t')$ in Eq. (1) other than the external shear stress $\pm F$. This noise term represents the effect of thermal fluctuations in the dislocation theory. Figure 3(c) shows the time evolution of the x coordinate of the vortex position at $D = 7.3\times10^{-5}$ and 0.094 for $F = 0.1018$. As D increases, the number of steps within the fixed time interval increases, however, the stick-slip motion is still observed.

Figure 4(a) shows the average velocity of the vortex motion as a function of F at $K = 1$, 2, and 4 for $d = 0.2$. The average velocity is determined by the average slope of the relationship between the time and the x coordinate of the vortex position. At $K = 1$, the vortex begins to move at $F > 1.002$, and the transition is continuous. At $K = 2$ and 4, the transition is discontinuous, and the hysteresis is observed. The origin of the hysteresis is not understood well. Figure 4(b) shows the critical force F_c for the stationary vortex to move as a function of K. The dashed line is $F_c = 0.1K$. $F_c = 0.1K$ is much smaller than the critical value $F_c = K$ of the desynchronization shown in Fig. 1. The critical value for the vortex motion takes almost the same value $F_c = 0.2$ when d is changed as $d = 0.1$, 0.2, 0.3, and 0.4 for $K = 2$, however, $F_c = 0.086$ at $d = 0$ for $K = 2$. The critical value becomes smaller when the viscosity is sufficiently small.

We have studied the vortex motion more in case of $d = 0$ more in detail. When $d = 0$, the total energy

$$E = \sum_{i,j} \frac{1}{2}\left(\frac{d\phi_{i,j}}{dt}\right)^2 - \frac{1}{2}\sum_{i,j}\sum_{i',j'} \cos(\phi_{i',j'} - \phi_{i,j})$$

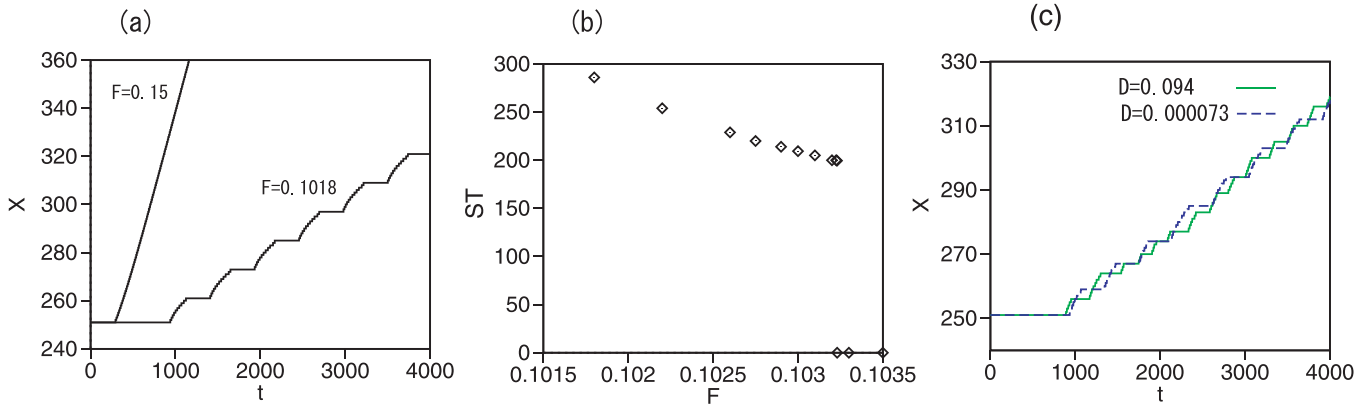

FIG. 3. (a) Time evolution of the x coordinate of the dislocation position at $F = 0.1018$ and 0.15 for $K = 1$ and $d = 0.2$. (b) Relationship between F and the stick time ST for $K = 1$ and $d = 0.2$. (c) Time evolution of the x coordinate of the vortex position at $F = 0.1018$ for $D = 7.3\times10^{-5}$ and 0.094 for $K = 1$.

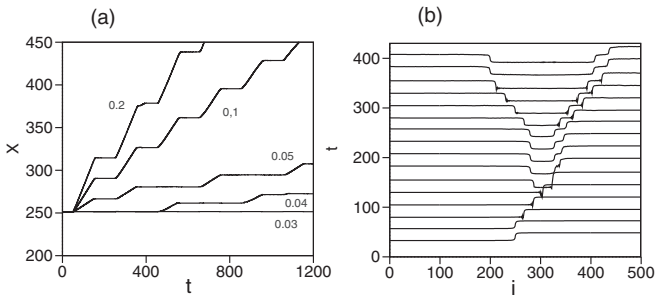

FIG. 5. (a) Time evolutions of the position of the vortex at $F = 0.03$, 0.04, 0.05, 0.1, and 0.2 for the conservative system of $d = 0$ and $K = 1$. (b) Time evolution of $\phi(i, j)$ at $j = L_y/2$ at $F = 0.3$, $K = 1$, and $d = 0$.

is conserved. Figure 5(a) shows the time evolution of the vortex position at $F = 0.03$, 0.04, 0.05, 0.1, and 0.2 for $d = 0$ and $K = 1$. The dislocation begins to move at $F = 0.038$ for $d = 0$. The slip-stick motion is observed for a wide parameter range of F. The slip motion starts at almost the same times for $F = 0.1$ and 0.2. The period is around 200. Even at $F = 0.03$, there is an oscillatory motion of very small amplitude with the period of around 200. Figure 5(b) shows the time evolution of $\phi(i, j)$ at $j = L_y/2$ at $F = 0.3$. A vortex-antivortex pair is created near $t = 120$, and the antivortex moves in the $-x$ direction. For a larger value of F, many vortex-antivortex pairs are created and chaotic motion appears. The proliferation of vortices is an interesting phenomenon, which is analogous to the proliferation dislocations in the problem of the plastic flow in solids.

Next, we have performed numerical simulations of the collision of the vortex and antivortex by imposing the periodic boundary conditions in the x direction because we need not consider the mirror image of vortices in the periodic boundary conditions. The periodic boundary conditions are imposed at $i = 1$ and L_x in a rectangular system of $L_x \times L_y$, and a vortex and antivortex are initially set at $i = 50$ and 150 in a system of 200×100. The no-flux boundary conditions are assumed at $j = 1$ and $j = L_y$. This type of boundary condition is used only in this numerical simulation. Figure 6 shows the numerical result at $F = 0.25$ for $K = 1$ and $d = 0.05$. Figure 6(a) shows the time evolutions of $\phi(i, j)$. A pair annihilation is observed, and a uniform state appears after the collision. Figure 6(b) shows a snapshot profile of $(\cos\phi_{i,j}, \sin\phi_{i,j})$ at $t = 220$ before the pair annihilation, and Fig. 6(c) shows a snapshot profile at $t = 240$ after the pair annihilation. Figure 7 shows the numerical result at $F = 0.3$. Figure 7(a) shows the the time evolutions of $\phi(i, j)$. The vortex and antivortex pass through each other at $F = 0.3$. The passing phenomenon of the vortex and antivortex is a phenomenon found in our model. Figure 7(b) shows a snapshot profile of $(\cos\phi_{i,j}, \sin\phi_{i,j})$ at $t = 175$ before the collision, and Fig. 7(c) shows a snapshot profile at $t = 180$ after the collision. In a very narrow parameter range above the critical line, a bound state of vortex and antivortex is generated. Figure 8(a) shows the time evolution of $\phi(i, j)$ at $F = 0.27$ for $K = 1$ and $d = 0.05$. At this parameter, the vortex and antivortex make a bound state after the collision. Figure 8(b) shows the stationary configuration of $(\cos\phi_{i,j}, \sin\phi_{i,j})$ near the vortex pair. The vortex locates at $x = 102.5$ and the antivortex locates at $x = 98.5$.

Figure 8(c) shows the critical line below which the pair annihilation occurs in a parameter space of (d, F) at $K = 1$. When d is larger than the critical value for a fixed value of F, pair annihilation occurs at the collision. When F is smaller than the critical value for a fixed value of d, the pair annihilation occurs at the collision. Even for $d = 0$, there is a transition from the pair annihilation to passing at $F = 0.205$ when F is increased as shown in Fig. 8(c).

Even in the case of no-flux boundary conditions, the collision between the vortex and antivortex is important. At $d = 0.2$ and $K = 1$, a single moving vortex disappears at the boundary, which can be interpreted as the pair annihilation of the vortex and antivortex locating at the mirror image of the original vortex. For a smaller value of d, the pair annihilation does not occur, and the two vortices with different signs pass through each other at the boundary. Figure 9(a) shows the time evolution of x coordinate of the vortex at $d = 0.01$ and $F = 0.4$. As an initial condition, one vortex is set at the center of the 500×100 system. The single vortex exhibits a reciprocal motion in the x direction. The vortex of the positive sign moves in the x direction, and

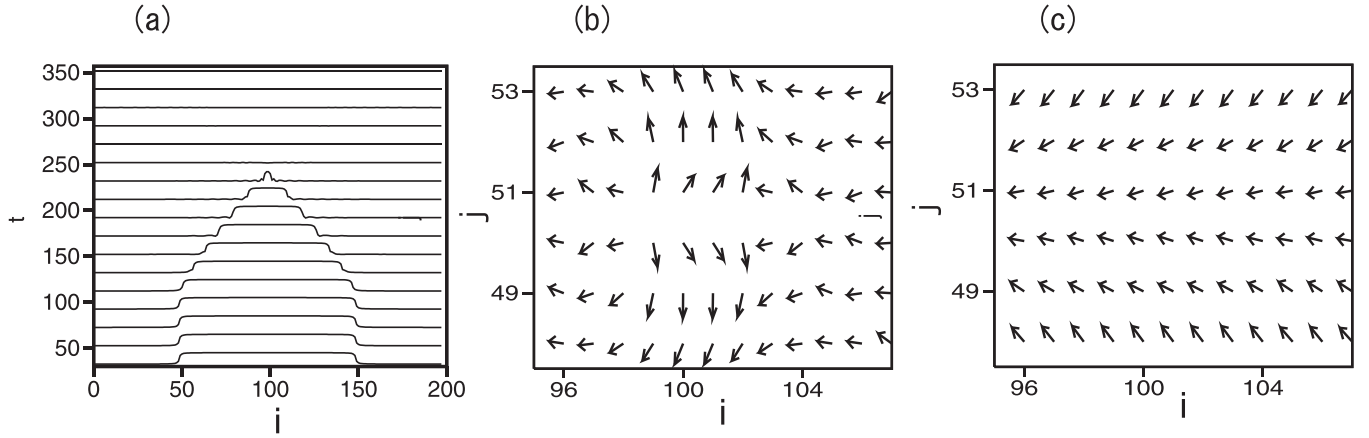

FIG. 6. (a) Time evolutions of $\phi(i, j)$ at $j = L_y/2$ at $F = 0.25$ for $K = 1$ and $d = 0.05$. (b) Snapshot profile of $(\cos\phi_{i,j}, \sin\phi_{i,j})$ at $t = 220$ before the pair annihilation. (c) Snapshot profile of $(\cos\phi_{i,j}, \sin\phi_{i,j})$ at $t = 240$.

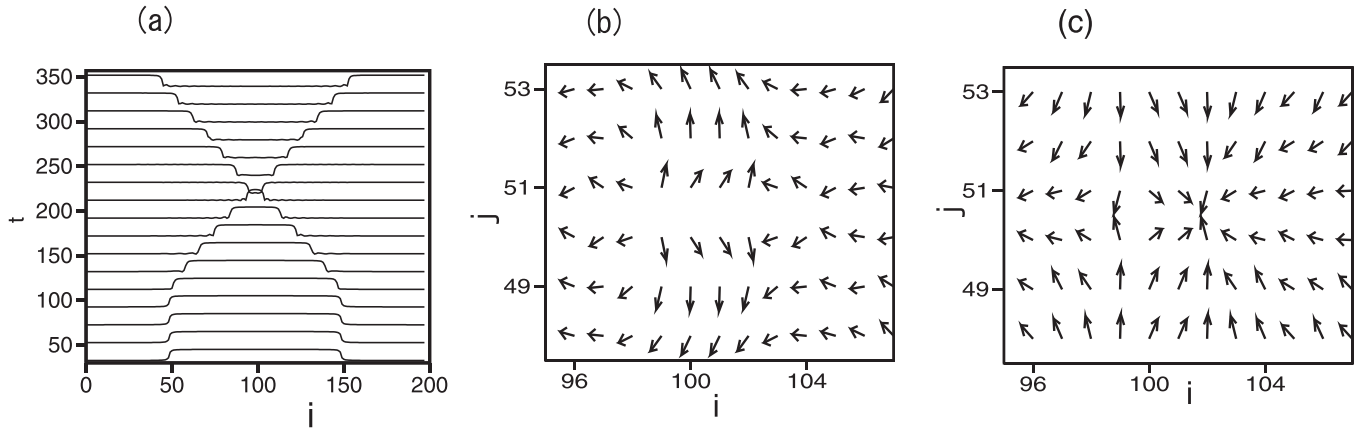

FIG. 7. (a) Time evolutions of $\phi(i, j)$ at $j = L_y/2$ at $F = 0.3$ for $K = 1$ and $d = 0.05$. (b) Snapshot profile of $(\cos\phi_{i,j}, \sin\phi_{i,j})$ at $t = 175$ before the collision. (c) Snapshot profile of $(\cos\phi_{i,j}, \sin\phi_{i,j})$ at $t = 180$.

the sign change occurs at the boundary $x = L_x$ and moves in the $-x$ direction. The y coordinate remains $j = L_y/2$. Figure 9(b) shows the time evolution of $\phi_{i,j}$ for $i = 100$ and $i = 300$ at $j = 74$. When the vortex passes through $(i, L_y/2)$, $\phi_{i,j}$ jumps by π for $j > L_y/2$, and $\phi_{i,j}$ jumps by $-\pi$ for $j < L_y/2$. Figure 9(c) shows the average frequency $\omega_j = (1/L_x)\sum_{i=1}^{L_x}\{\phi_{i,j}(10\,000) - \phi_{i,j}(5000)\}/5000$. There is a jump in the average frequency ω at $j = L_y/2$. This implies the desynchronization between the phase oscillators in the upper region $j > L_y/2$ and the ones in the lower regions $j < L_y/2$. The frequency ω is around 0.038 for $i > L_x/2 + 1$, which is equal to the $2\pi/T$, where $T = 1645 = 2L_x/v$ is the time for the reciprocating motion of the vortex between 0 and L_x. If $\phi_{i,j} = 0$ and there is no vortex at $t = 0$, the desynchronization does not occur until $F = 1$ for $K = 1$. Figure 9 implies that the existence of the vortex induces desynchronization. If $\phi_{i,j}$ is interpreted to be the displacement in the z direction, the desynchronization corresponds to the plastic flow where the upper and lower regions of a solid move in the opposite directions. The vortex motion plays an essential role in the desynchronization, which corresponds to the dislocation motion in the plastic flow in solids.

For larger F, the pair creation of vortices occurs frequently. Figure 10(a) shows the time evolution of x coordinate of vortices of positive or negative sign at $d = 0.01$, $K = 1$, and $F = 0.5$. The number of vortices changes in time by the pair creation and annihilation of vortices. Figure 10(b) shows the time evolution of y coordinate of vortices. The y coordinates change in time; however, they are distributed near $L_y/2$. Figure 8(c) shows the average frequency $\omega_j = (1/L_x)\sum_{i=1}^{L_x}\{\phi_{i,j}(10\,000) - \phi_{i,j}(5000)\}/5000$. Owing to the phase slips by the vortex motion, ω takes a different value between the upper and lower regions. The frequency profile changes smoothly as a function of j in contrast to the sharp transition shown in Fig. 9(c). This is because the vortex position is distributed around $L_y/2$, owing to the chaotic vortex dynamics. The average frequency $\bar{\omega}$ calculated by the spatial average of ω_j for $j > 3L_y/4$ is evaluated at 0.0181 at $F = 0.5$. On the other hand, the temporal average of the vortex number is 5.18 at $F = 0.5$. Both the average frequency $\bar{\omega}$ and average vortex number at $F = 0.5$ are around five times larger than the case of $F = 0.4$. Figure 10(d) shows a relationship between the average number N of vortices and the frequency $\bar{\omega}$ obtained by changing F at $K = 1$ and $d = 0.01$. The dashed line

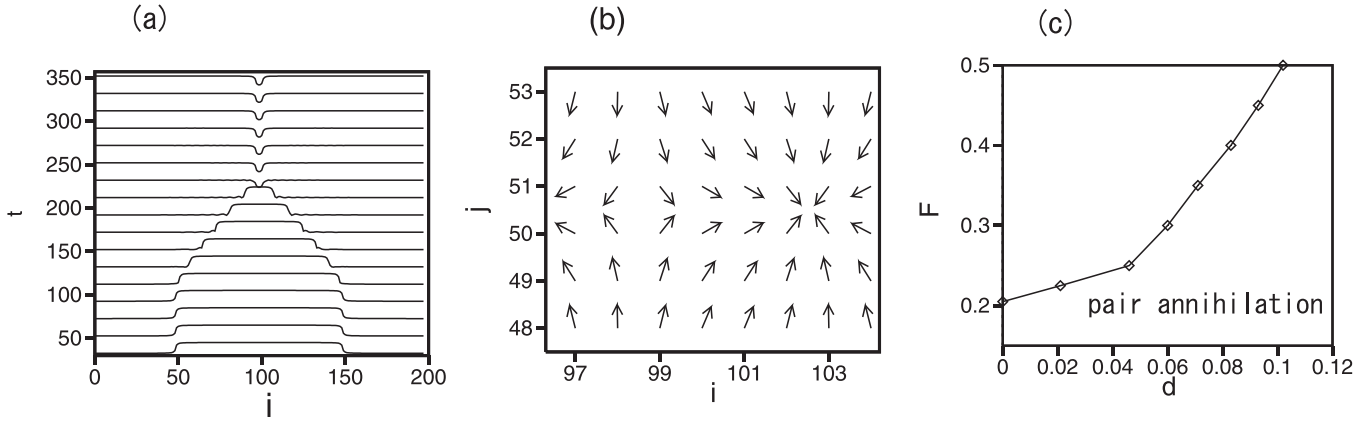

FIG. 8. (a) Time evolutions of $\phi(i, j)$ at $j = L_y/2$ at $F = 0.27$ for $K = 1$ and $d = 0.05$. (b) Stationary profile of $(\cos\phi_{i,j}, \sin\phi_{i,j})$ at $F = 0.27$. (c) Critical line below which the pair annihilation occurs in a parameter space (d, F) $K = 1$.

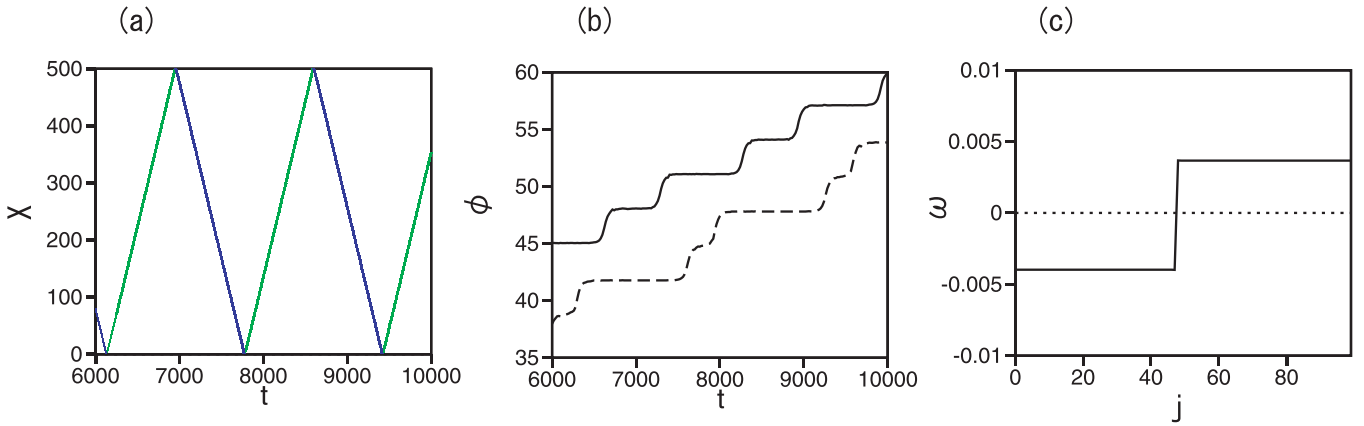

FIG. 9. (a) Time evolution of the x coordinate of the vortex at $d = 0.01$ and $F = 0.4$. (b) Time evolution of $\phi_{i,j}$ for $i = 300$ (solid line) and 100 (dashed line) at $j = 74$. (c) Frequency ω_j as a function of $j - L_y/2$ at $F = 0.4$ and $d = 0.01$.

is the linear approximation $\bar{\omega} = 0.035N$, although there is no mathematical analysis now. The frequency increases with the vortex number because $\phi_{i,j}$ jumps by π for $j > L_y/2$ when a vortex passes through a point (i, j_0) satisfying $j_0 < j$. In any case, it has been shown that the vortex dynamics is directly related to the frequency distribution of the phase oscillators.

III. COMPLEX DYNAMICS OF VORTEX LINES IN THREE DIMENSIONS

A three-dimensional phase model of vortex dynamics is expressed as

$$\frac{d^2\phi_{i,j,k}}{dt^2} = K\sum_{i',j'} \sin(\phi_{i',j',k'} - \phi_{i,j,k}) - d\frac{d\phi_{i,j,k}}{dt} + f_{i,j,k}, \tag{5}$$

where (i', j', k') is the sixth-nearest-neighbor site of the (i, j, k) site on the cuboid lattice of $L_x \times L_y \times L_z$. The no-flux boundary conditions are imposed at $i = 1$, $i = L_x$, $j = 1$, L_y, $k = 1$, and $k = L_z$. A vortex ring is set at $j = L_y/2$ as an initial condition to study the dynamics of the vortex ring. The external force is assumed to be $f_{i,j,k} = F$ at $j = L_y$, $f_{i,j,k} = -F$ at $j = 1$, and $f_{i,j,k} = 0$ for the other sites.

The numerical simulation was performed in a cubic lattice of $80 \times 80 \times 80$. Figure 11 is five snapshot patterns of the vortex ring at $t = 0$, 10, 20, 30, and 40 in a cross section of $j = L_y/2$ for $K = 1$, $d = 0.3$ and $F = 0.3$. Figure 11 shows the time evolution that the vortex ring expands, collides with the boundaries, and disappears at $d = 0.3$. Although the vortex ring disappears at the boundaries for $d \geqslant 0.05$ at $K = 1$ and $F = 0.3$, the reflection of vortex lines occurs for $d < 0.05$, which is similar to the two-dimensional system.

Figure 12 shows numerical results at $d = 0.03$ and $F = 0.43$. Figure 12(a) shows the time evolution of the total number S of elemental square loops with nonzero vorticity. Here, the elemental square loop is $(i, j, k) \to (i + 1, j, k) \to (i + 1, j + 1, k) \to (i, j + 1, k) \to (i, j, k)$, $(i, j, k) \to (i, j + 1, k) \to (i, j + 1, k + 1) \to (i, j, k + 1) \to (i, j, k)$, and $(i, j, k) \to (i, j, k + 1) \to (i + 1, j, k + 1) \to (i + 1, j, k) \to (i, j, k)$. The vorticity is calculated from the summation of the phase difference: $\sum(\phi_{i',j',k'} - \phi_{i,j,k})$ along the elemental square loop. The summation takes 0, 2π, or -2π, and the vorticity is defined by the summation divided by 2π. S is the total number of the elemental square loops with nonzero vorticity. For $F = 0.43$ and $d = 0.03$, a fairly regular oscillation of S is observed in the numerical simulation of Eq. (5). The number S roughly represents the length of the vortex ring. At the parameters, the vortex ring expands and collides with the boundaries. The vortex ring is reflected at the boundaries and shrinks. Figure 12(b) shows four half rings moving toward the center at $t = 525$ after the reflection

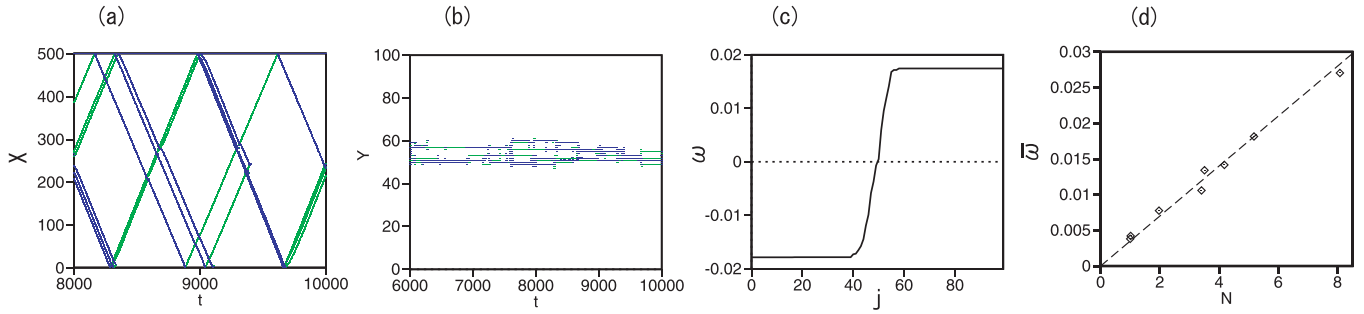

FIG. 10. (a) Time evolution of the x coordinate of the vortex at $d = 0.01$ and $F = 0.5$. (b) Time evolution of the y coordinate of the vortex at $d = 0.01$ and $F = 0.4$. (c) Frequency ω_j as a function of j at $F = 0.5$ and $d = 0.01$. (d) Relationship between the average number of vortices and the average frequency $\bar{\omega}$ obtained by changing F at $K = 1$ and $d = 0.01$. The dashed line is $\bar{\omega} = 0.035N$.

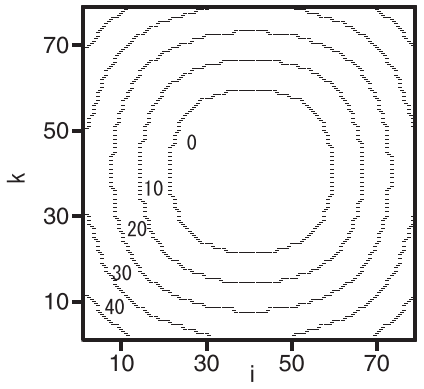

FIG. 11. Five snapshot patterns of the vortex ring at $t = 0$, 10, 20, 30, and 40 in the section of $j = L_y/2$ for $d = 0.3$ and $F = 0.3$.

at the boundaries. The four half rings collide with each other, and a reconnection of vortex lines occurs between $t = 525$ and 530. Figure 12(c) shows a snapshot of the vortex lines at $t = 530$ after the reconnection.

For larger F, creation and annihilation of vortex lines occur, and the dynamics become chaotic. Figure 13 shows numerical results at $d = 0.012$, $K = 1$, and $F = 0.5$. Figure 13(a) shows a snapshot of vortex line. Complicated vortex lines are observed. Figure 13(b) shows the time evolution of S. Chaotic time evolution of S is observed by the chaotic creation and annihilation of vortex lines. Figure 13(c) shows of the frequency $\omega_j = 1/(L_x L_z) \sum_{k=1}^{L_z} \sum_{i=1}^{L_x} \{\phi_{i,j,k}(1500) - \phi_{i,j,k}(750)\}/750$. The vortex lines are localized near $j = L_y/2$ and the frequency profile has a jump around $j = L_y/2$. The average frequency takes almost the same value in the two regions $j > L_y/2$ and $j < L_y/2$, and the profile of the frequency changes rapidly near $j = L_y/2$. That implies that the upper and lower regions are desynchronized because the phase slips occur near $j = L_y/2$ by the vortex motion. Figure 13(d) shows a relationship between S and the average frequency $\bar{\omega}$ for $55 \leqslant j \leqslant 80$ obtained by changing F for $0.35 \leqslant F \leqslant 0.5$ at $K = 1$ and $d = 0.012$. The average frequency increases with S; that is, the desynchronization develops with the multiplication of vortex lines. Thus, we have found the desynchronization induced by vortex lines even in the three-dimensional systems.

IV. CREATION OF VORTICES AND VORTEX LINES BY IMPURITIES

It is known that impurities play an important role in the dislocation motion and plastic flows in solids. In the previous sections, we studied homogeneous phase oscillator lattices. In this section, we study the effect of impurities in the phase oscillator lattices. A two-dimensional phase oscillator lattice with inhomogeneity in the coupling constant is expressed as

$$\frac{d^2\phi_{i,j}}{dt^2} = \sum_{i',j'} K_{r',r} \sin(\phi_{i',j'} - \phi_{i,j}) - d\frac{d\phi_{i,j}}{dt} + f_{i,j}, \qquad (6)$$

where (i', j')'s are the four nearest-neighbor sites of the (i, j) site on the square lattice of $L_x \times L_y$, and $K_{r'r}$ is the coupling constant between the (i', j') and (i, j) sites. The no-flux boundary conditions are imposed at $i = 1$, $i = L_x$, $j = 1$, and L_y. In Sec. II, a single vortex or a pair of vortices was set as an initial condition. In this section, we will show the creation of vortices from a uniform state owing to the impurities. Therefore, $\phi_{i,j} = 0$ and $d\phi_{i,j}/dt = 0$ are assumed as an initial condition. The coupling constant $K_{r',r}$ is 1 except for the impurity. We will show that a pair of vortices is spontaneously created around the impurity when F is increased. We have performed numerical simulations in a system where the coupling constant $K_{r',r}$ locally takes a different value from 1. Figure 14(a) shows the time evolution of the total vortex number when the coupling constant is 0.2 in the circular region of $(i - L_x/2)^2 + (j - 3L_y/4)^2 < 9$ at $F = 0.75$ and $d = 0.4$. The number of oscillators in this circular region is 29. Figure 14(a) shows the time evolution of the vortex number. A pair of vortex and antivortex appears first at $t \simeq 1424$ near $i = L_x/2$ and $j = 3L_y/4 + 3$, which is the top site of the circular region, and the vortex number jumps from 0 to two. The vortex moves to the right and disappears at the boundary $x = L_x$, the antivortex moves to the left and

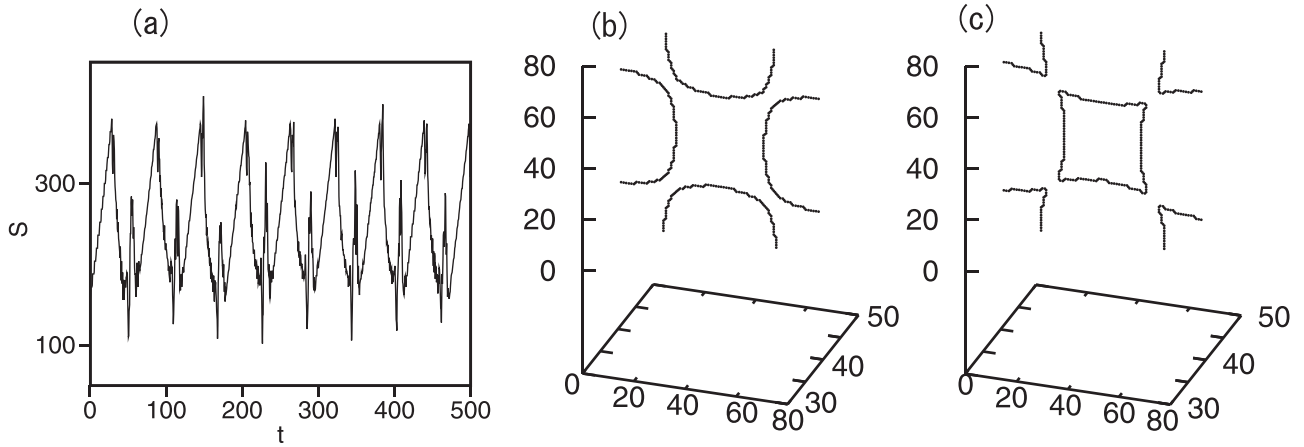

FIG. 12. Numerical results of the three-dimensional model at $d = 0.03$ and $F = 0.43$. (a) Time evolution of the total number S of elemental square loops with nonzero vorticity. (b) Snapshot of vortex lines at $t = 525$. (c) Snapshot of vortex lines at $t = 530$.

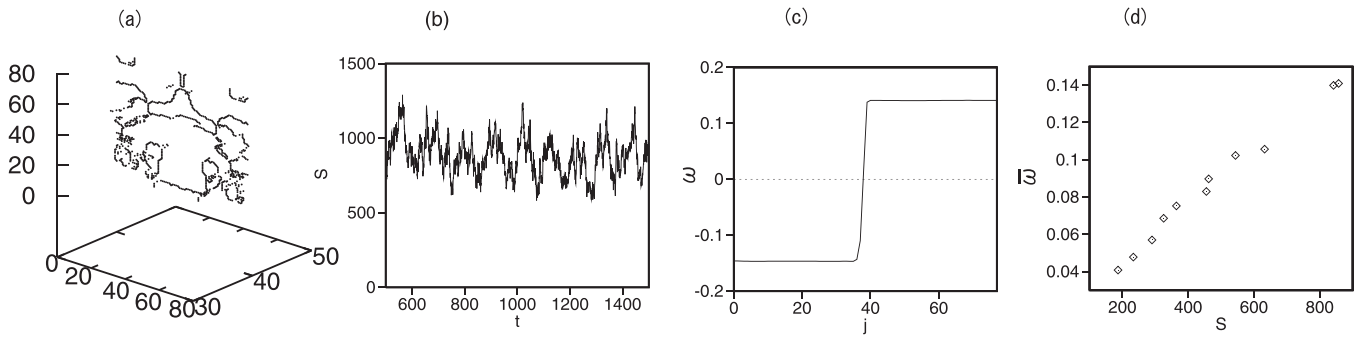

FIG. 13. Numerical results of the three-dimensional model at $d = 0.012$ and $F = 0.5$. (a) Snapshot of vortex lines at $t = 750$. (b) Time evolution of S. (c) Frequency ω_j as a function of j. (d) Relationship between S and the average frequency $\bar{\omega}$ for $55 < j < 80$ obtained by changing F for $0.35 \leqslant F \leqslant 0.5$ at $K = 1$ and $d = 0.012$.

disappears at $x = 0$, and the vortex number becomes 0. After a while, a new vortex pair is created again near $i = L_x/2$ and $j = 3L_y/4 + 3$. The creation of the vortex pair and the annihilation at the boundaries repeats periodically with period T. Figure 14(b) shows the frequency $\omega = 2\pi/T$ of the oscillation of vortex number as a function of F. The pair creation occurs for $F > 0.71$ at $d = 0.4$, and the frequency increases continuously from 0. The disappearance of the vortex and antivortex at the no-flux boundaries is due to the large value of d. For smaller d, the annihilation of the vortex at the boundaries does not occur, and many vortices can be created, as shown in Figs. 9 and 10. Figure 11(c) shows the chaotic time evolution of the vortex number at $F = 0.75$ and $d = 0.05$ for the same configuration of the coupling constant K.

In three dimensions, a vortex ring can be spontaneously created in inhomogeneous systems. The three-dimensional phase oscillator lattice with inhomogeneous coupling constant is expressed as

$$\frac{d^2\phi_{i,j,k}}{dt^2} = \sum_{i',j',k'} K_{r',r} \sin(\phi_{i',j',k'} - \phi_{i,j,k}) - d\frac{d\phi_{i,j,k}}{dt} + f_{i,j,k}, \tag{7}$$

where (i', j', k')'s are the six nearest-neighbor sites of the (i, j, k) site on the cubic lattice of $L\times L\times L$, and $K_{r'r}$ is the coupling constant between the (i', j', k') and (i, j, k) sites. The no-flux boundary conditions are imposed at $i = 1$, $i = L$, $j = 1$, $j = L$, $k = 1$, and $k = L$. Similarly to the two-dimensional system, $\phi_{i,j,k} = 0$ and $d\phi_{i,j,k}/dt = 0$ are assumed as an initial condition. The external force is applied only at $j = 1$ and $j = L$ as $f_{i,1,k} = -F$ and $f_{i,L,k} = F$ as the shear stress, and $f_{i,j,k}$ is set to 0 for the other sites. The coupling constant $K_{r',r}$ is set to be 1 except for impurities. As an example, $K_{r',r}$ is assumed to be 6 in a spherical region of $(i - L/2)^2 + (j - 5L/8)^2 + (k - L/2)^2 < 25$ for $L = 80$. The number of oscillators in this spherical region is 498. The parameter d is set to be $d = 0.5$.

Figure 15(a) is the time evolution of the total number S of elemental square loops with nonzero vorticity at $F = 0.9$ for $d = 0.5$. S represents roughly the length of the vortex ring. A vortex ring appears near $t = 650$, the radius of the vortex ring increases, and the vortex ring collides with the boundary and disappears owing to the large value of d. The creation and annihilation of a vortex ring repeat in time. Figure 15(b) shows three snapshots of the vortex ring at $t = 2190$, 2220, and 2250. The spreading process of the vortex ring is observed. The creation of the vortex ring occurs for $F \geqslant 0.685$ at $d = 0.5$ and $L = 80$. Figure 15(c) is the frequency ω of the oscillation of S when F is changed. The frequency increases continuously from 0 at $F \simeq 0.685$ at $d = 0.5$.

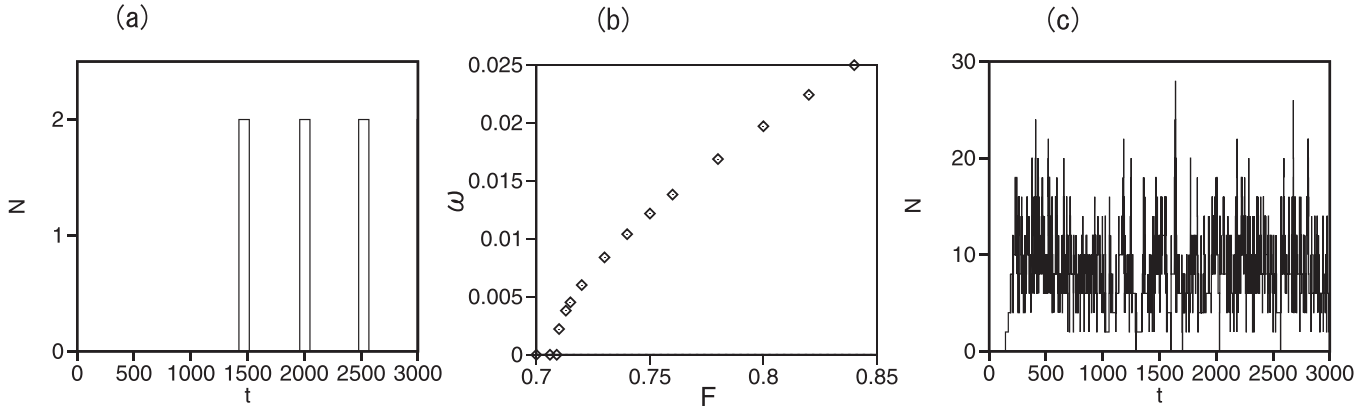

FIG. 14. (a) Time evolution of the vortex number at $F = 0.75$ and $d = 0.4$. (b) Frequency of the oscillation of vortex number as a function of F at $d = 0.4$. (c) Time evolution of the vortex number at $F = 0.75$ and $d = 0.05$.

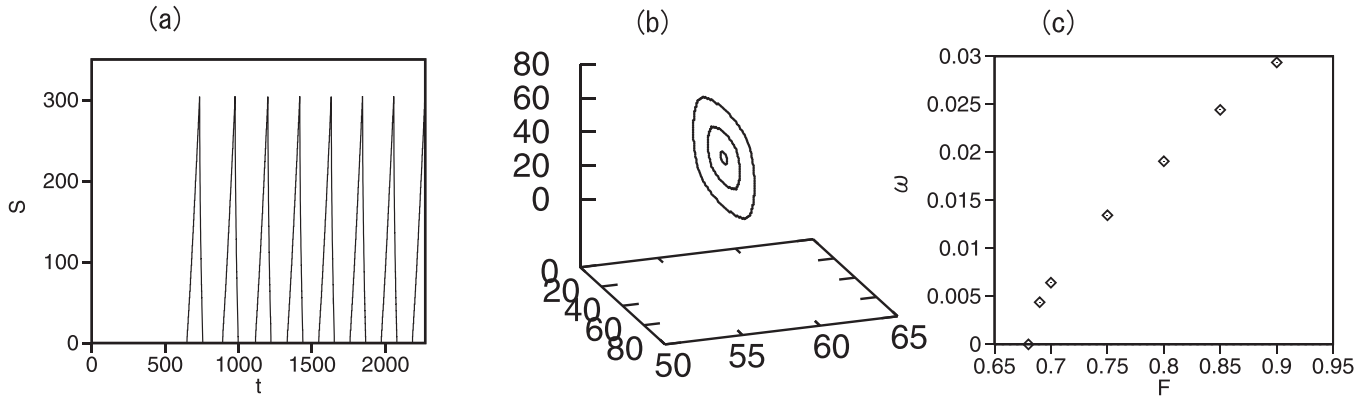

FIG. 15. (a) Time evolution of S of the vortex ring at $d = 0.5$ and $F = 0.9$. (b) Three snapshots of the vortex ring at $t = 2190$, 2220, and 2250. (c) Frequency ω of the oscillation of S as a function of F for $d = 0.5$.

V. INTERACTION BETWEEN VORTEX LINE AND IMPURITIES

It is known that impurities can trap a dislocation, and impurities' suppression of the dislocation motion can harden the material in the theory of plasticity. We will show a numerical simulation of the interaction of the moving vortex line with an impurity region. The system size is $L\times L\times L = 100\times 100\times 100$. As an initial condition, a straight vortex line is set at $i = L/4$ and $j = L/2$. The vortex line moves in the x direction at $F = 0.2$ for $d = 0.1$. In a spherical impurity region of $(i - L/2)^2 + (j - L/2)^2 + (k - L/2) < 9$, the coupling constant is assumed to be $K(r', r) = 6$. In the other region, the coupling constant is 1. Figure 16(a) shows the time evolution of $\phi(i, j, k)$ at $j = L/2$ and $k = L/2$. $\phi_{i,j,k}$ exhibits a jump at the vortex position. Figure 16(a) shows that the vortex line moves in the x direction; it is once trapped in the impurity region, and then the vortex line moves in the x direction again. Figure 16(b) shows the time evolution of the total number S of elemental square loops with nonzero vorticity. The vortex line is deformed by being trapped in the impurity region, and S increases. After the vortex line passes through the impurity region, S decreases by recovering the straight vortex line. The vortex line moves toward the boundary $x = L$ and disappears. A vortex ring remains around the impurity region, and S keeps a nonzero value $S = 32$. Figure 16(c) shows the three snapshots of vortex lines at $t = 175$, 300, and 400. At $t = 300$ (green), the vortex line is deformed by the impurity region, At $t = 400$ (red), the deformed vortex line is split into a vortex ring around the impurity region and a vortex line. This trapping process of the vortex line is similar to the Orowan mechanism in the dislocation theory. When the dislocation line passes through an impurity region in solids, a dislocation loop called the Orowan loop is left behind around the impurity region, which is similar to the process shown in Fig. 16. The Orowan mechanism is important because it is closely related to the dispersion hardening of materials.

VI. SUMMARY

We have proposed a phase oscillator lattice with inertia and studied the complex dynamics of vortex points and vortex lines as an analog of the dislocation motion in solids under the shear stress. We have numerically found various dynamical phenomena. The vortex begins to move if the shear stress is beyond a critical force, which corresponds to the Peierls stress in the dislocation theory. We have numerically found that the vortex exhibits a stick-slip motion for sufficiently

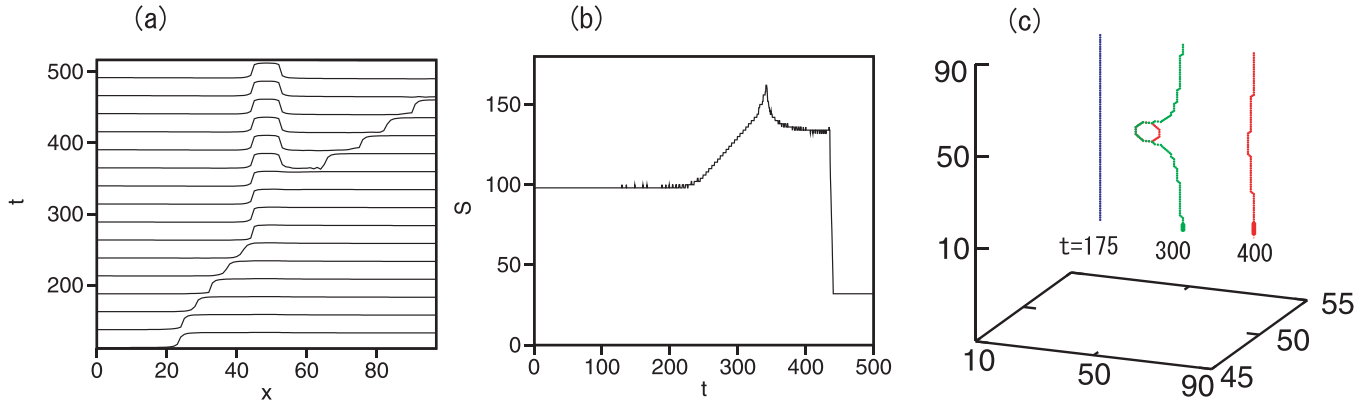

FIG. 16. (a) Time evolution of $\phi_{i,j,k}$ at the section of $j = L/2$ and $k = L/2$ for $L = 100$ at $d = 0.1$ and $F = 0.2$, and $L = 100$. The vortex line is initially set at $i = L/4$ and $j = L/2$ and an impurity region of radius 3 is set at the center $i = L/2$, $j = L/2$, and $k = L/2$. (b) Time evolution of the length S of the vortex ring at $d = 0.1$ and $F = 0.2$, and $L = 100$. (c) Three snapshots of the vortex lines at $t = 175$, 300, and 400.

small d. The pair annihilation of vortex and antivortex occurs for large d and the vortices pass through for small d, when F is fixed. There is a transition from the pair annihilation to passing when F is increased for a fixed value of d. The transition occurs even for $d = 0$. The passing phenomenon of the vortex and antivortex is a finding in our model. Owing to the passing phenomenon, a single vortex can exhibit a reciprocal motion in a system of the no-flux boundary conditions, and the frequency jump appears on the line where the vortex exhibits the reciprocal motion in the x direction. When F is larger for small d, many vortex pairs are spontaneously created, and chaotic behaviors appear. We have found that the frequency jump at the phase slip region increases with the number of spontaneously generated vortices. The desynchronization induced by the vortex motion is the main result of this paper. The desynchronization induced by the vortex lines was also found in the three-dimensional oscillator lattices. The desynchronization in the phase oscillator lattices corresponds to the plastic flow via the dislocation motion in solids.

We have also studied the effect of inhomogeneity in the coupling constant. A vortex pair or a vortex ring is periodically created around the impurity region even when the initial condition is uniform. Finally, we have found that a vortex loop remains after the vortex line passes through an impurity region. This corresponds to the Orowan loop in the dislocation theory.

Although our phase oscillator lattice model is much simpler than the models studied in the dislocation theory, our model can reproduce several important properties of dislocation motions. Complex vortex dynamics can be more easily studied in our model, which has not been studied well in the dislocation theory.

We have numerically found various interesting phenomena in the coupled phase oscillator lattices with inertia; however, the theoretical understanding of the phenomena is not sufficient. Since our model is a dynamical system of many degrees of freedom, mathematical analysis is not easy. Even in a system of a single or two vortices, there are nontrivial phenomena such as the stick-slip motion and the transition from the pair annihilation to passing. We would like to develop some mathematical analyses of the model equation in the future.

[1] Y. Kuramoto, *Chemical Oscillations, Waves, and Turbulence* (Springer, New York, 1984).

[2] A. Pikovsky, M. Rosenblum, and J. Kurths, *Synchronization: A Unified Concept in Nonlinear Sciences* (Cambrdge University Press, Cambridge, 2001).

[3] J. A. Acebrón, L. L. Bonilla, C. J. Perez Vincente, F. Ritort, and R. Spigler, Rev. Mod. Phys. **77**, 137 (2005).

[4] H. Sakaguchi and Y. Kuramoto, Prog. Theor. Phys. **76**, 576 (1986).

[5] S. H. Strogatz, Physica D **143**, 1 (2000).

[6] E. Ott and T. M. Antonsen, Chaos **18**, 037115 (2008).

[7] Y. Kuramoto, *International Symposium on Mathematical Problems in Theoretical Physics*, edited by H. Araki, Lecture Notes in Physics, Vol. 39 (Springer, Berlin, Heidelberg, 1975), p. 420.

[8] H. A. Tanaka, A. J. Lichtenberg, and S. Oishi, Phys. Rev. Lett. **78**, 2104 (1997).

[9] F. Dörfler and F. Bullo, SIAM J. Appl. Dyn. Syst. **10**, 1070 (2011).

[10] H. Sakaguchi and T. Matsuo, J. Phys. Soc. Jpn. **81**, 074005 (2012).

[11] H. Sakaguchi, S. Shinomoto, and Y. Kuramoto, Prog. Theor. Phys. **77**, 1005 (1987).

[12] H. Hong, H. Chate, H. Park, and L. H. Tang, Phys. Rev. Lett. **99**, 184101 (2007).

[13] H. Sakaguchi, S. Shinomoto, and Y. Kuramoto, Prog. Theor. Phys. **79**, 1069 (1988).

[14] W. T. Read, *Dislocations in Crystals* (McGraw Hill, New York, 1953).

[15] A. H. Cottrell, *Dislocations and Plastic Flow in Crystals* (Oxford University Press, New York, 1953).

[16] B. Devincre and M. Condat, Acta Metall. Mater. **40**, 2629 (1992).

[17] K. W. Schwarz, J. Appl. Phys. **85**, 108 (1999).

[18] Y. Frenkel and T. Kontorova, Zh. Eksp. Teor. Fiz. **8**, 89 (1938).

[19] O. M. Braun and Y. S. Kivshar, Phys. Rep. **306**, 1 (1998).

[20] J. Norell, A. Fasolino, and A. S. de Wijn, Phys. Rev. E **94**, 023001 (2016).